Hindawi Publishing Corporation
Journal of Materials
Volume 2013, Article ID 716452, 9 pages
http://dx.doi.org/10.1155/2013/716452

Research Article

Absorption and Radiation Transitions in $Mn^{2+}(3d^5)$ Configuration of Mn-Doped ZnS Nanoparticles Synthesized by a Hydrothermal Method

Bui Hong Van,[1] Pham Van Ben,[1] Tran Minh Thi,[2] and Hoang Nam Nhat[3]

[1] *Hanoi University of Science, Vietnam National University, Vietnam*
[2] *Hanoi National University of Education, Vietnam*
[3] *University of Engineering and Technology, Vietnam National University, Vietnam*

Correspondence should be addressed to Tran Minh Thi; tranminhthi@hnue.edu.vn

Received 1 January 2013; Revised 18 March 2013; Accepted 22 March 2013

Academic Editor: Maurizio Ferrari

The Mn-doped ZnS nanoparticles with Mn content of 0–15 mol% were synthesized by a hydrothermal method from the solutions $Zn(CH_3COO)_2$ 0.1 M, $Mn(CH_3COO)_2$ 0.01 M, and $Na_2S_2O_3$ 0.1 M at 220°C for 15 h. These nanoparticles presented the cubic structure with average particle size about 16 nm. The yellow-orange photoluminescence (PL) band at 586 nm was attributed to the radiation transition of the electrons in $3d^5$ unfilled shell of Mn^{2+} ions [$^4T_1(^4G)$-$^6A_1(^6S)$] in ZnS matrix. The photoluminescence excitation (PLE) spectra monitored at the yellow-orange band, the absorption spectra also showed the near band edge absorption of 336–349 nm and the characteristic absorption bands of $Mn^{2+}(3d^5)$ ions at 392, 430, 463, 468, 492, and 530 nm. These bands should be attributed to the absorption transitions of $3d^5$ electrons from the ground state $^6A_1(^6S)$ to the excited states $^4E(^4D)$, $^4T_2(^4D)$, $^4A_1(^4G)$-$^4E(^4G)$, $^4T_2(^4G)$, and $^4T_1(^4G)$ of Mn^{2+} ions. The intensity of PL band and absorption bands of $Mn^{2+}(3d^5)$ ions also increased with the Mn content from 0.1 to 9 mol%, but their peak positions were almost unchanged. The PLE spectra showed clearly the energy level splitting of Mn^{2+} ions in ZnS crystal field and allowed for the calculation of the splitting width between the excited states $^4A_1(^4G)$, $^4E(^4G)$ about of 229 cm^{-1} (28.6 meV), and the Racah parameters $B = 559\ cm^{-1}$, $C = 3202\ cm^{-1}$ ($\gamma = C/B = 5.7$), and the crystal field strength $D_q = 568\ cm^{-1}$. The PL spectra with different excitation wavelengths corresponding to absorption transition bands of the PLE spectra allow for the discussion of the indirect and direct excitation mechanisms of $Mn^{2+}(3d^5)$ ions in the ZnS crystal.

1. Introduction

In the Mn-doped A^2B^6 semiconductor crystals such as ZnS, ZnSe, and CdTe the energy levels ^6S, ^4G, ^4P, and ^4D of Mn^{2+} ions with a $3d^5$ unfilled electronic shell (called the $Mn^{2+}(3d^5)$ configuration) are splitted into the multiple levels $^6A_1(^6S)$, $^4T_1(^4G)$, $^4T_2(^4G)$, $^4E(^4G)$, $^4A_1(^4G)$, $^4T_2(^4D)$, and $^4E(^4D)$ under the crystal field of the host matrix. The splitting of these energy levels has been studied both theoretically and experimentally [1–7]. Tanabe and Sugano have calculated the energy levels of $Mn^{2+}(3d^5)$ configuration in the octahedral crystal field and obtained the energy levels diagram representing the dependence of the E/B ratio on Δ_0/B (which corresponds with $C = 4.77B$ [4]), where E is the energy of the terms of the free $Mn^{2+}(3d^5)$ ions, Δ_0 is the crystal field splitting energy, B and C are the Racah parameters characterizing the interaction between the $3d^5$ electrons of Mn^{2+} ions, and D_q is the crystal field strength. Fazzio and coworkers have calculated the energy structure of the $Mn^{2+}(3d^5)$ ions in a tetrahedral crystal field of ZnS crystal particularly and determined the splitting width of ^4G state of about 3242 cm^{-1} (402 meV) and the energy splitting width of two very near energy levels $^4E(^4G)$ and $^4A_1(^4G)$ of about 390 cm^{-1} (48.4 meV) [5]. Based on the PLE spectra monitored at the yellow-orange band, the groups of Chen et al. [6, 7] determined the Racah parameters B, C and crystal

field strength D_q by the following formulas:

$$\begin{aligned} 10B + 5C &= E_1, \\ 100D_q^2 - \left(14B + 5C - E_2\right)\left(22B + 7C - E_2\right) &= \frac{12B^2\left(E_2 - 22B - 7C\right)}{13B + 5C - E_2}, \\ 17B + 5C &= E_3, \end{aligned} \tag{1}$$

where E_1, E_2, and E_3 are the photon energies characterizing the absorption transition of electrons from the ground state $^6A_1(^6S)$ to the excited states $^4A_1(^4G)$-$^4E(^4G)$, $^4T_2(^4G)$, and $^4E(^4D)$ of $Mn^{2+}(3d^5)$ ions in ZnS crystals, respectively. These results were calculated for bulk material: $B = 609\,cm^{-1}$, $C = 3111\,cm^{-1}$ ($\gamma = C/B = 5.1$), and $D_q = 667\,cm^{-1}$; for nanomaterials with particle size of 3.5, 4.5, and 10 nm, B = 490, 551, 521 cm^{-1}; C = 3357, 3246, 3306 cm^{-1} ($\gamma = C/B$ = 6.8; 5.9; 6.3); D_q = 586, 600, and 637 cm^{-1}, respectively. However, the calculated results of these parameters for Mn-doped ZnS materials were only determined when the $Mn^{2+}(3d^5)$ ions were well substituted into the positions of the $Zn^{2+}(3d^{10})$ ions. In this work, we systematically study the effect of Mn content on the absorption and radiation transitions of electrons in the $Mn^{2+}(3d^5)$ configuration of Mn-doped ZnS nanoparticles synthesized by a hydrothermal method with a large range of Mn content from 0.1 mol% to 15 mol% using S^{2-} from $Na_2S_2O_3$. The Racah parameters B, C and the crystal field strength D_q are calculated from the experimental results, and then the discussions are presented about the excitation mechanism of $Mn^{2+}(3d^5)$ ions in the ZnS crystal at the increasing Mn content based on the dependence of PL spectra on excitation wavelengths.

2. Experimental

2.1. Synthesis of the Mn-Doped ZnS Nanoparticles. The Mn-doped ZnS nanoparticles (called ZnS:Mn nanoparticles) with different Mn contents were synthesized by the hydrothermal method according to the following process. The initial solutions $Zn(CH_3COO)_2$ 0.1 M (A), Mn $(CH_3COO)_2$ 0.01 M (B) were mixed together in the specified molar ratios to obtain 30 mL of solution (C) and stirred for 60 minutes. Then, $Na_2S_2O_3$ 0.1 M solution (D) with the volume of 30 mL was slowly dropped into solution (C) with continuous stirring for 60 minutes. This final mixture was put into the teflon-lined chamber steel vessel with a closed lid, after being annealed at 220°C for 15 h and cooled down to room temperature naturally. In the hydrothermal process, the ZnS nanocrystals were formed as follows:

$$\begin{aligned} 4Na_2S_2O_3 &\longrightarrow Na_2S + 3Na_2SO_4 + 4S \\ Zn(CH_3COO)_2 + Na_2S &\longrightarrow ZnS\downarrow + 2CH_3COONa \end{aligned} \tag{2}$$

Besides ZnS, the small portion of MnS was also formed:

$$Mn(CH_3COO)_2 + Na_2S \longrightarrow MnS\downarrow + 2CH_3COONa \tag{3}$$

As these two processes happened simultaneously, the Mn-doped ZnS nanoparticles were believed to be formed as a final product. In fact, the host material ZnS might exhibit defects associated with Zn or S vacancies or surface and interstitial defects. The obtained precipitation was filtered, washed by distilled water, and dried at 60°C for 10 h in ambient condition. By the above process, the Mn-doped ZnS nanoparticles were synthesized in the powder form with the different Mn contents of 0, 0.1, 0.4, 1, 2, 4, 6, 8, 9, 10, and 15 mol%.

2.2. Structural and Optical Measurements. The crystal structure was studied by the X-ray diffraction method (XRD) on the XD8-Advance Buker system with Cu-Kα radiation (λ = 1.54056 Å). The surface morphology was examined using the transmission electron microscope (TEM) JEM-1010. The PL and PLE spectra were recorded at 300 K using the 325 nm excitation radiation of a He-Cd laser, radiation of XFOR-450 xenon lamp on the Oriel-Spec MS-257, FL3-22 spectrometers, respectively. The absorption spectra were examined by the reflection-scattering process and recorded at 300 K using radiation of detri, halogen lamp on Jasco-V670 spectrometer.

3. Results and Discussion

3.1. The Structure and Morphology of ZnS:Mn Nanoparticles. Figure 1 shows the XRD patterns of ZnS, ZnS:Mn nanoparticles with different Mn contents. This patterns consists of the diffraction lines corresponding to the reflecting planes (111), (200), (220), and (311) in which the (111) line is the strongest. The obtained pattern demonstrate that the ZnS, ZnS:Mn nanoparticles possess a single-phase cubic structure with $T_d^2 - F\bar{4}3m$ symmetry and calculated lattice constant of ZnS a = 5.413 Å. This value is in good agreement with the lattice constant from JCPDS card number 05-0566 (a = 5.406 Å). For the ZnS:Mn nanoparticles with Mn contents of 0.1, 0.4 mol%, the lattice constant was unchanged a = 5.404 Å. For the ZnS:Mn nanoparticles with Mn content from 1 to 15 mol%, the lattice constant increased slightly from 5.414 to 5.439 Å. This increase may be explained by that the ionic radius of Mn^{2+} was larger than that of Zn^{2+} 10% [8] and indicated that the $Mn^{2+}(3d^5)$ ions were really substituted for $Zn^{2+}(3d^{10})$ sites. Based on the Debye-Scherrer's formula

$$D = \frac{0.9\lambda}{\beta\cos\theta}, \tag{4}$$

where D (Å) is the particle size, λ (Å) is the X-ray wavelength of Cu-Kα, β (rad) is the full width at half maximum (FWHM) of the diffraction line, and θ (rad) is the Bragg angle, the average sizes of the nanoparticles were calculated to be about 16 nm. This value did not vary with Mn content from 0.1 to 15 mol%.

Figure 2 shows the TEM images of ZnS:Mn nanoparticles with Mn contents of 0.1, 9 mol%. They showed that the nanoparticles are the quasi-spheres with average size of about 25–43 nm. Thus, this value is bigger than particle size calculated from Debye-Sherrer's formula because of the aggregation of ZnS:Mn crystals.

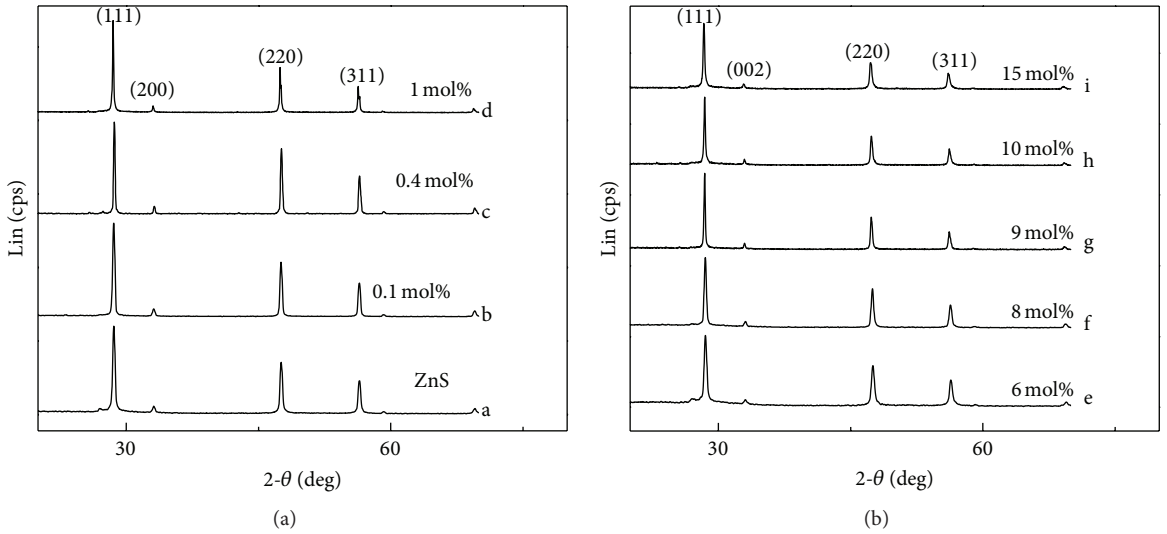

Figure 1: XRD patterns of the ZnS:Mn nanoparticles with different Mn contents.

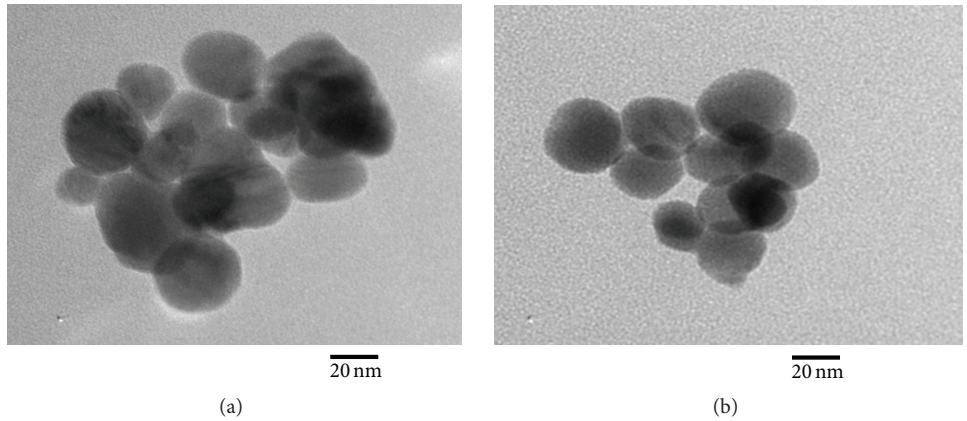

Figure 2: TEM images of ZnS:Mn nanoparticles with Mn contents of (a) 0.1 mol% and (b) 9 mol%.

3.2. The Absorption and Radiation Transitions in the $Mn^{2+}(3d^5)$ Configuration of ZnS:Mn Nanoparticles. The radiation transitions in the $Mn^{2+}(3d^5)$ configuration were examined by the PL spectra according to Mn content, a power density, and a wavelength of the excitation radiation. Simultaneously, the absorption transitions in this configuration were studied by the PLE and absorption spectra. Figure 3 shows the PL spectra of ZnS, ZnS:Mn nanoparticles with different Mn contents. As seen, the PL spectrum of ZnS nanoparticles shows a wide blue band of about 450 nm (Figure 3(a)). This band is attributed to the origin of the Zn, S vacancies and their interstitial atoms in the host ZnS crystal [9–14]. For the samples with Mn content of 0.1 mol%, the blue band was almost quenching, but its PL spectra exhibited a broad yellow-orange band at 586 nm (Figure 3(b)) which should be characterized by the radiation transition of electrons in the $Mn^{2+}(3d^5)$ configuration $[^4T_1(^4G) \rightarrow {}^6A_1(^6S)]$ [15]. Besides, for the samples with Mn content from 0.4 to 9 mol%, the substitution of $Mn^{2+}(3d^5)$ ions into the $Zn^{2+}(3d^{10})$ sites increased, so the PL intensity of the yellow-orange band gradually increased and achieved the maximum with Mn content of 9 mol% while peak position was unchanged (Figures 3(c)–3(h)). By contrast, for the samples with Mn contents of 10, 15 mol%, the intersite interaction is possible between the Mn^{2+} ions themselves and between them and other ions in the lattice, so the intensity of the yellow-orange PL decreased (Figures 3(i) and 3(j)) [8, 16, 17]. The dependence of the yellow-orange PL intensity on Mn content is shown in Figure 4.

The unchanged position and the increase of yellow-orange PL intensity were also observed with increasing power density of 325 nm excitation radiation from 0.10 to 0.27 W/cm^2 (Figure 5). Based on the relationship between the PL intensity I_{PL} and the excitation power density I_{EX} by equation:

$$I_{PL} = kI_{EX}^{n}, \tag{5}$$

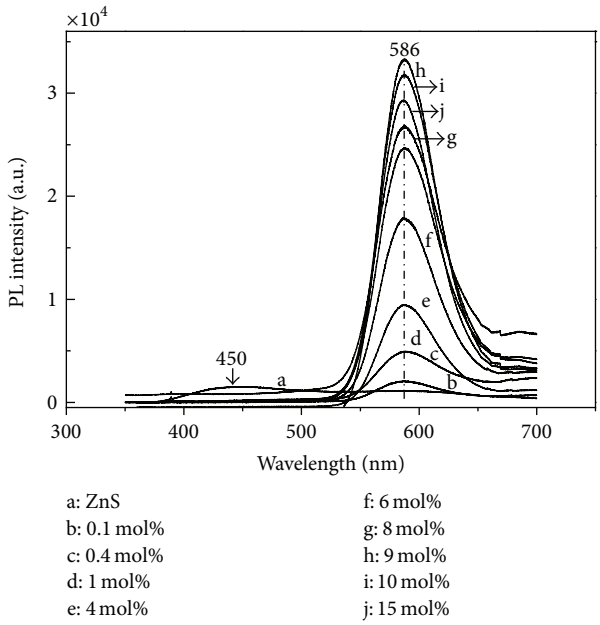

Figure 3: The PL spectra of the ZnS:Mn nanoparticles with different Mn contents.

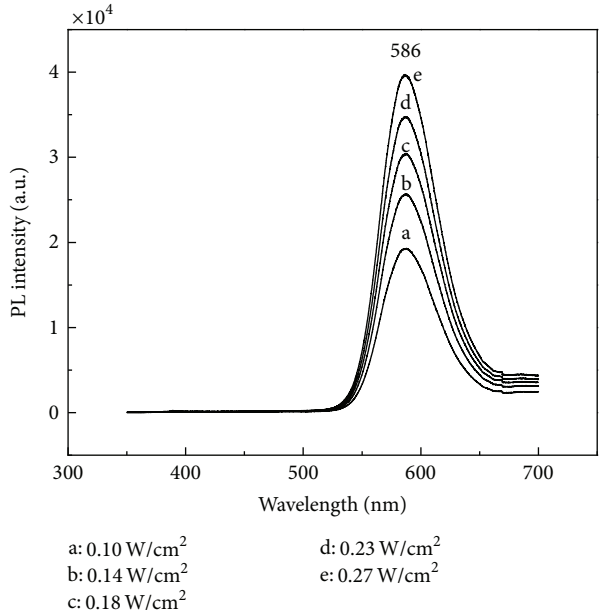

Figure 5: The PL spectra of ZnS:Mn nanoparticles for Mn content of 9 mol% with different excitation power densities.

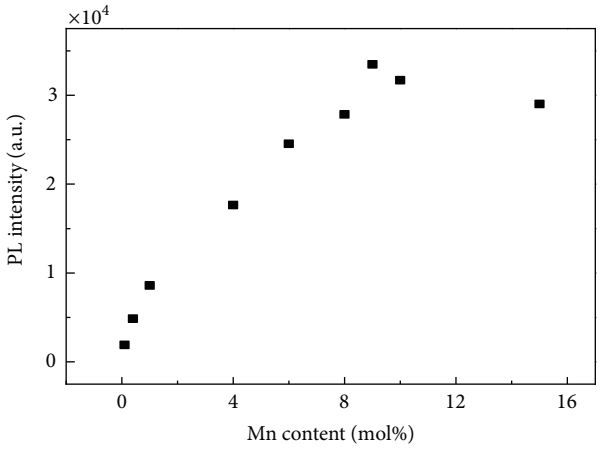

Figure 4: The dependence of the yellow-orange PL intensity of ZnS:Mn nanoparticles on Mn content.

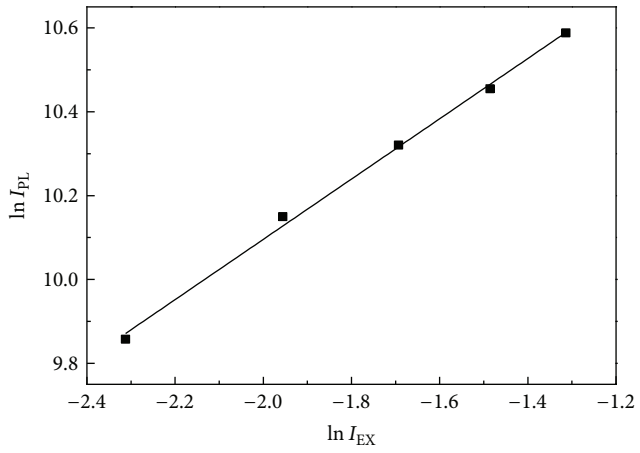

Figure 6: The dependence of $\ln I_{PL}$ on $\ln I_{EX}$ of the yellow-orange PL intensity for ZnS:Mn nanoparticles with Mn content of 9 mol%.

where k is a constant, n is the coefficient dependent on radiation mechanism, the n value was determined to be approximately 1 (Figure 6). This result agrees well with the radiation mechanism of impurity center in ZnS crystal [18]. This suggested that the yellow-orange PL was a characteristic radiation transition of electrons in the $3d^5$ unfilled shell of $Mn^{2+}(3d^5)$ ions in ZnS crystals.

Figure 7 shows the PLE spectra monitored at the yellow-orange PL band excited by the radiation from a xenon lamp. For the ZnS:Mn nanoparticles with Mn contents of 0.1, 0.4 mol%, there was a wide range with strong PL intensity at 336 nm (3.691 eV) which was characteristic for the near band edge absorption of the ZnS crystals because the photon energy corresponding to this transition is near the width of band gap [12, 19]. Besides, these PLE spectra also showed the bands with smaller PL intensity at 392, 430, 468, 492, and 530 nm (Figures 7(a) and 7(b)), which were attributed to the absorption transitions of the $3d^5$ electrons from the ground state $^6A_1(^6S)$ to the excited states $^4E(^4D)$, $^4T_2(^4D)$, $^4A_1(^4G)$-$^4E(^4G)$, $^4T_2(^4G)$, and $^4T_1(^4G)$ of $Mn^{2+}(3d^5)$ ions, respectively [7].

For the ZnS:Mn nanoparticles with Mn content increased from 1 to 15 mol%, the PL band characterized to the near band edge absorption was shifted towards the longer wavelength from 342 to 349 nm (Figures 7(c)–7(h)). This shift might be caused by the s-d exchange interaction of the conduction

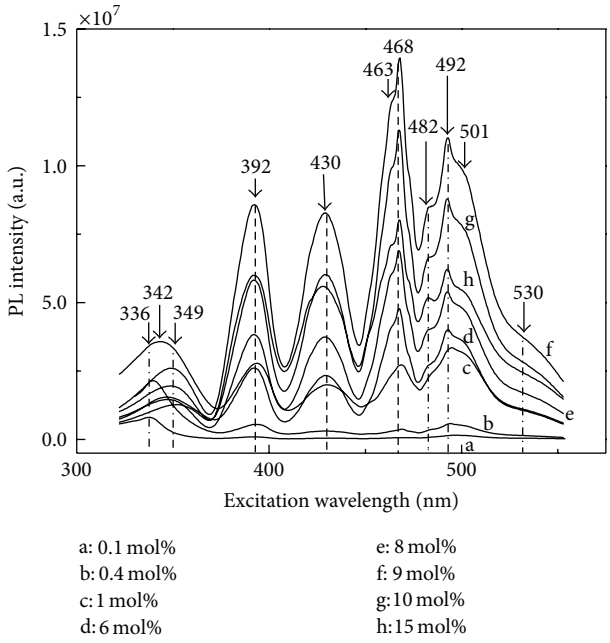

FIGURE 7: The PLE spectra monitored at the yellow-orange PL band of ZnS:Mn nanoparticles with different Mn contents.

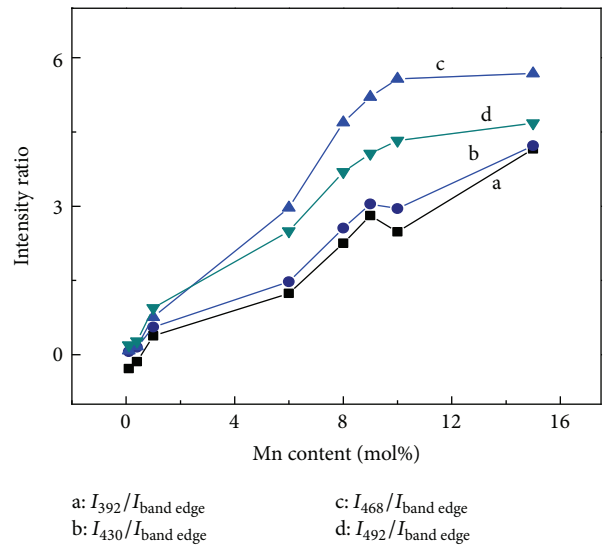

FIGURE 8: The PL intensity ratio dependence of $Mn^{2+}(3d^5)$ absorption transition bands and near band edge absorption transition band on different Mn contents.

electrons with the $3d^5$ electrons of Mn^{2+} ions. Due to this interaction, the band gap decreased slightly when Mn content increased [20, 21]. However, the PL intensity of Mn^{2+} absorption transition bands in the PLE spectra increased with increasing of Mn content from 0.1 to 8 mol% (Figures 7(a)–7(e)) and reached the maximum at 9 mol% (Figure 7(f)), then decreased again at 10 and 15 mol% (Figures 7(g) and 7(h)) but their peak positions were almost unchanged. This result agreed quite well with the observed PL spectra. Although the PL intensity of the Mn^{2+} absorption transition bands varied up and down with Mn content, in general the PL intensity ratio of Mn^{2+} absorption transition bands and the near band edge absorption transition band increased (Figure 8). This shows that the $Mn^{2+}(3d^5)$ ions were doped into the crystal lattice at $Zn^{2+}(3d^{10})$ sites, including their vacancies sites, so the probability of the occurrence of near band edge absorption decreased while the probability of occurrence of absorption in the $Mn^{2+}(3d^5)$ configuration increased.

The detailed study about 468 nm (2.650 eV) band in the PLE spectra showed that the peak of 463 nm (2.678 eV) appeared unclearly in the left shoulder of this band for ZnS:Mn samples with Mn contents of 0.1, 0.4, 1 mol% (Figures 7(a)–7(c)) and more clear for the Mn content from 6 to 15 mol% (Figures 7(d)–7(h)). The bands at 463 and 468 nm were attributed to the absorption transitions of the electrons from the ground state $^6A_1(^6S)$ to the excited states $^4A_1(^4G)$ and $^4E(^4G)$ of $Mn^{2+}(3d^5)$ ions, respectively. The energy difference between these excited states is about 229 cm^{-1} (28.6 meV) and the splitting energy gap for the ^4G state of $Mn^{2+}(3d^5)$ ions is around 2734 cm^{-1} (339 meV). This value agrees well with the result of the calculation provided by Fazzio and coworkers and by the experiment of MnS material (about 200 cm^{-1} (24.8 meV)) [5]. Similar results were obtained for the $Mn^{2+}(3d^5)$ absorption band at the range from 480 to 515 nm. For the ZnS:Mn samples with Mn contents of 0.1, 0.4, 1 mol%, a wide band appeared with a maximum at about 492 nm (Figures 7(a)–7(c)). For the ZnS:Mn samples with Mn content from 6 to 15 mol%, near the band at 492 nm, also the new bands at 482 and 501 nm appeared (Figures 7(d)–7(h)). Among them, the band at 492 nm is the characteristic absorption transition of the electrons from the ground state $^6A_1(^6S)$ to the excited state $^4T_2(^4G)$ of $Mn^{2+}(3d^5)$ ions. The calculated energy gaps between $^4T_2(^4G)$ state and states corresponding to the bands at 482 and 501 nm are 53.3 and 50.2 meV, respectively.

Using the photon energies of E_1, E_2, and E_3 corresponding to the wavelengths of 392, 468, and 492 nm in the PLE spectra monitored at the yellow-orange PL band of ZnS:Mn nanoparticles and (1), the Racah parameters and the crystal field strength were determined: $B = 559\ cm^{-1}$, $C = 3202\ cm^{-1}$, ($\gamma = C/B = 5.7$), and $D_q = 568\ cm^{-1}$. These values are in good agreement with parameters B, C, and D_q obtained for ZnS:Mn nanomaterials [7].

To clarify the absorption transitions in $Mn^{2+}(3d^5)$ configuration more, the absorption spectra of ZnS, ZnS:Mn samples were examined. Figure 9 shows the absorption spectra of these samples with different Mn contents. As seen, the absorption spectrum of ZnS nanoparticles appears as a wide band of about 334 nm with strong absorption (Figure 9(a)), which is attributed to the near band edge absorption of ZnS crystal [10]. For the ZnS:Mn samples with the Mn content from 0.1 to 15 mol%, the near band edge shifted to the longer wavelength at 337 nm (Figures 9(b)–9(i)). For the ZnS:Mn sample with Mn content of 8 mol%, besides that band, there appeared bands at 392, 429, 467, and 500 nm, in which the band at 467 nm was the strongest absorption (Figure 7(f)).

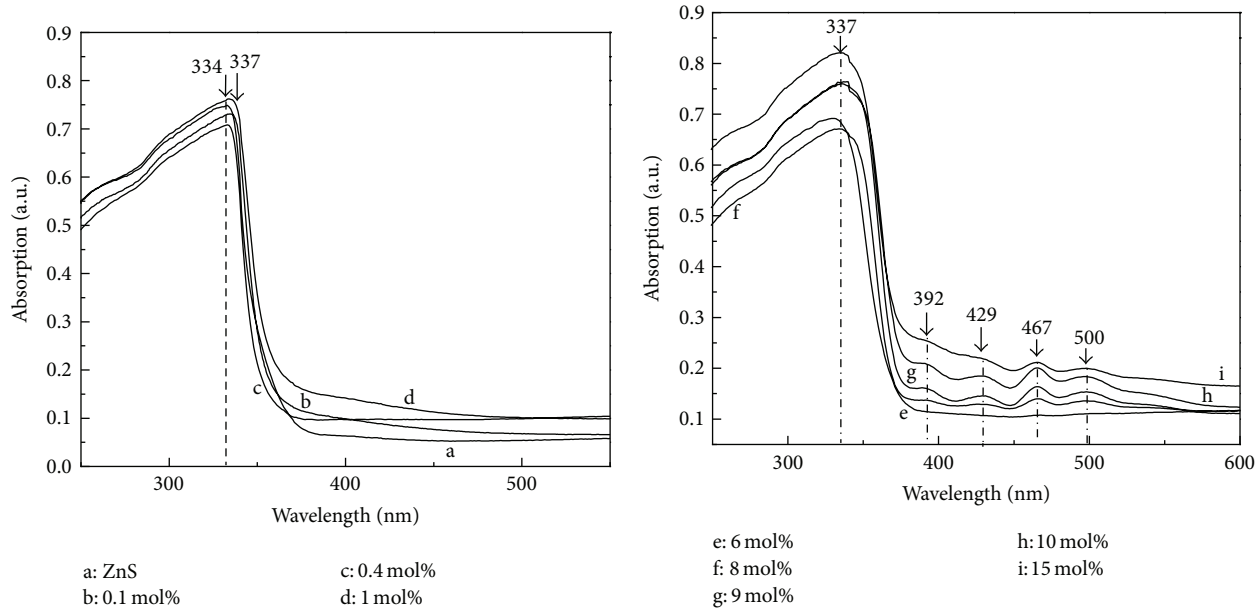

Figure 9: The absorption spectra of the ZnS:Mn nanoparticles with different Mn contents.

The positions of these bands were identical to the ones seen in the PLE spectra monitored at the yellow-orange band, but their absorptions were smaller because the PL bands in the PLE spectra were characteristic by the resonance absorption transitions of $Mn^{2+}(3d^5)$ ions. With the increase of Mn content from 9 to 15 mol%, their absorptions increased, but their peak positions remained unchanged (Figures 9(g)–9(i)). This suggested that these bands must also be characteristic by the absorption of $Mn^{2+}(3d^5)$ ions. Thus, the presence of $Mn^{2+}(3d^5)$ ions in ZnS host material has created a yellow-orange band at 586 nm in the PL spectra and bands at 392, 430, 463, 468, 492, and 530 nm in the PLE spectra and the absorption spectra. These peak positions were consistent with the positions of the emission bands of ZnS:Mn nanoparticles calculated from the Kohl-Sham Density Functional Theory equation [22].

In order to determine the excitation mechanism of $Mn^{2+}(3d^5)$ ions, the PL spectra of ZnS:Mn samples with Mn contents of 0.1, 1, 9, 15 mol% were investigated by different excitation wavelengths. Using in turn radiations of the xenon lamp corresponding to the wavelengths of 325, 336, 349, 392, 430, 468, and 492 nm in the PLE spectra to excite these ZnS:Mn samples, their PL spectra present only a yellow-orange band at 586 nm. This proved that even with small Mn content of 0.1 mol% the $Mn^{2+}(3d^5)$ ions were really substituted with the $Zn^{2+}(3d^{10})$ sites. The peak position of the yellow-orange band was almost unchanged but its intensity depended on the excitation wavelength. For the ZnS:Mn samples with Mn content of 0.1, 1 mol%, the PL intensity of yellow-orange band was strongest as excited by the wavelengths of 336, 349 nm, and then the intensity decreased gradually as excited by 325, 392, 492, 468, and 430 nm (Figures 10(a) and 10(b)). On the contrary, for ZnS:Mn samples with Mn contents of 9, 15 mol%, the PL intensity was the strongest as excited by the wavelength of 468 nm, and then it decreased gradually as excited by the wavelengths of 392, 492, 430, 349, 325 nm (Figures 10(c) and 10(d)). The obtained results showed that there might be two dominant excitation mechanisms for the $3d^5$ electrons of Mn^{2+} ions: (i) the indirect and (ii) the direct excitations [9]. The absorption and radiation transitions caused by the excitation radiation of 325, 336, and 349 nm with photon energy near the band gap energy of ZnS mainly belong to (i) the indirect excitation [19, 23].

Under radiation, the imbalance electron-hole pairs can be bound with the Mn^{2+} ions; these carrier pairs can recombine nonradiatively and transfer the energy to the $3d^5$ electrons of Mn^{2+} ions. However, the absorption and radiation transitions caused by 392, 492, 468, and 430 nm radiations with the photon energy smaller than the band gap of ZnS belong to the (ii) direct excitation [19, 23]. When the electrons in the $3d^5$ unfilled shell of the ion $Mn^{2+}(3d^5)$ absorb the photon, they may transfer from the ground state $^6A_1(^6S)$ to the excited states $^4E(^4D)$, $^4T_2(^4D)$, $^4A_1(^4G)$-$^4E(^4G)$, $^4T_2(^4G)$, and $^4T_1(^4G)$, from where they are transited nonradiatively down to the state $^4T_1(^4G)$ and eventually transit down the ground state $^6A_1(^6S)$ to emit the yellow-orange band at 586 nm. The absorption and radiation transitions of electrons in the unfilled $3d^5$ shell of Mn^{2+} ions in the ZnS crystals and excitation energy transfer mechanism are shown in Figure 11.

4. Conclusion

By the hydrothermal method we have successfully synthesized ZnS:Mn nanoparticles with Mn content variying in a wide range from 0.1 to 15 mol%, in which the $Mn^{2+}(3d^5)$ ions substituted well into ZnS matrix even at the Mn content of 0.1 mol%. The substitution of the $Mn^{2+}(3d^5)$ ions in

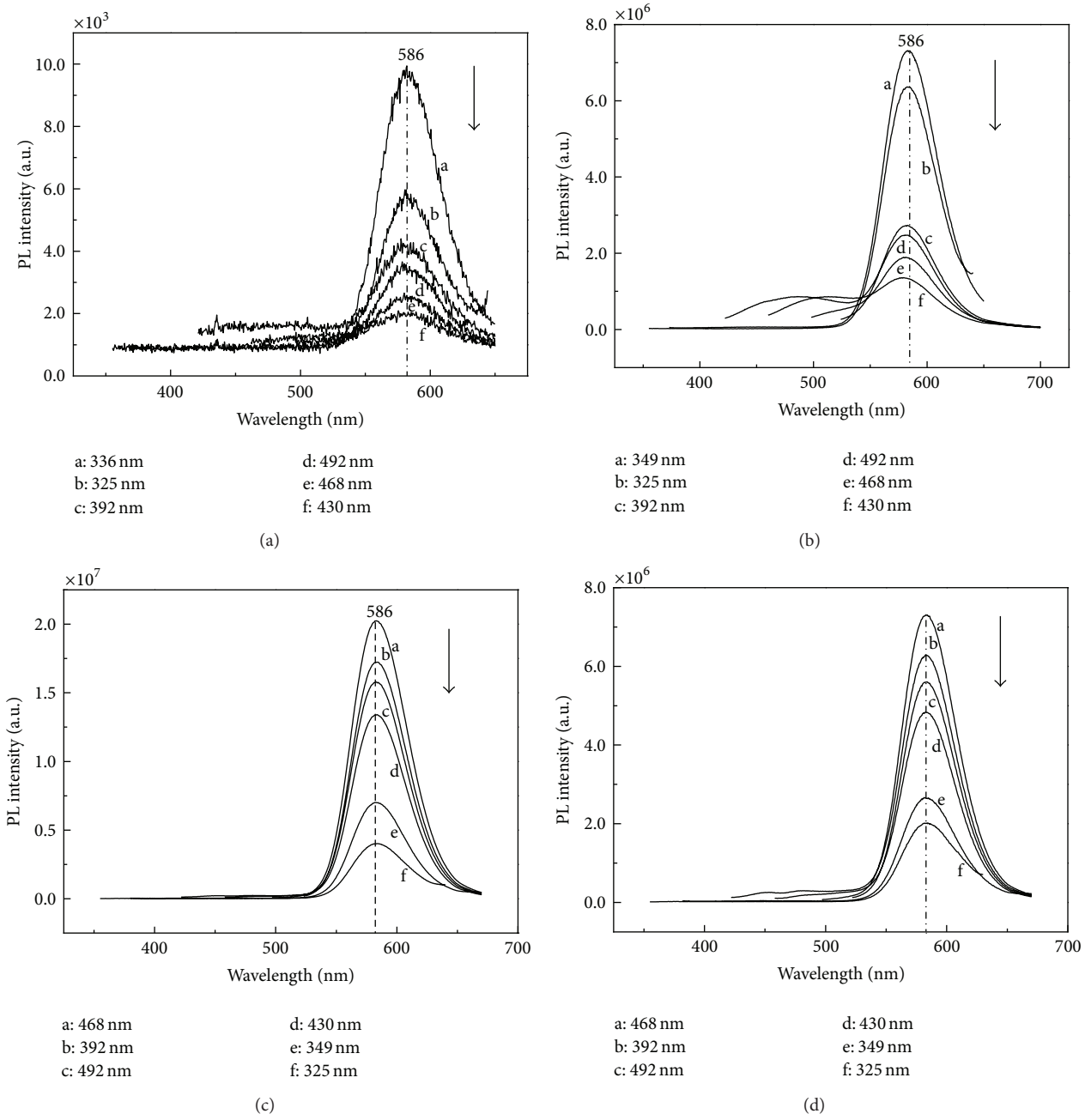

Figure 10: The PL spectra of ZnS:Mn nanoparticles with Mn contents of (a) 0.1 mol%, (b) 1 mol%, (c) 9 mol%, and (d) 15 mol% excited by different excitation radiations.

the positions of $Zn^{2+}(3d^{10})$ sites and their vacancies caused a small change in the lattice structure of the ZnS host material but affected significantly its optical behavior. The Mn^{2+} ions quenched the blue band at 450 nm and induced the appearance of a yellow-orange band at 586 nm in the PL spectra and the new bands at 392, 430, 463, 468, 492, and 530 nm in the PLE spectra and in the absorption spectra. When increasing the Mn content, the probability of absorption, radiation transitions in $Mn^{2+}(3d^5)$ ions increases, with the maximum at 9 mol% of Mn content after being reduced. Then, the energy level splitting of Mn^{2+} ions in ZnS crystal got more clear. The clear appearance of the absorption bands of $Mn^{2+}(3d^5)$ ions in the PLE spectra allows to determine the energy gap of two states $^4A_1(^4G)$, $^4E(^4G)$ about of 28.6 meV, the Racah parameters B, C, and the crystal field strength D_q. The unchanged yellow-orange PL peak position at 586 nm of the samples excited by different excitation wavelengths showed the presence of the indirect and direct excitation mechanisms for the $3d^5$ electrons of Mn^{2+} ions. When the Mn content increased from 0.1 to 15 mol%, the probability

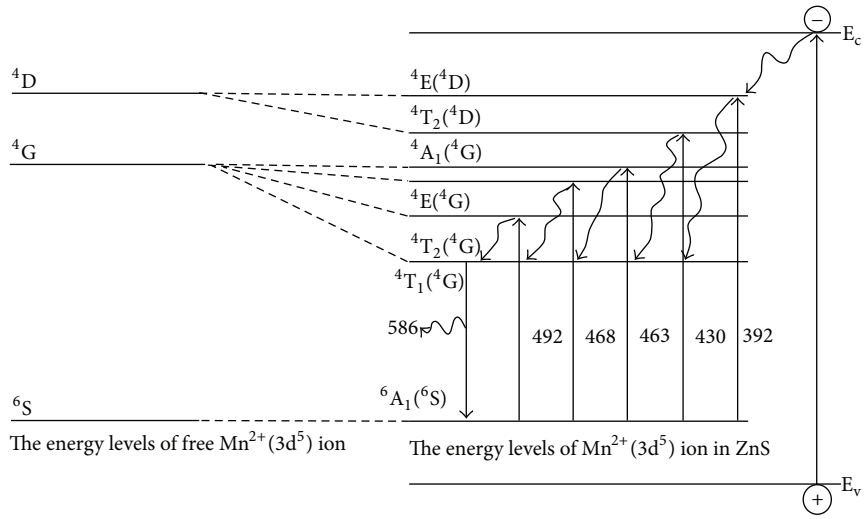

Figure 11: The energy levels diagram and the absorption radiation transitions of $Mn^{2+}(3d^5)$ ions in the ZnS:Mn crystal field.

of the indirect excitation decreased, while the one of direct excitation increased.

Acknowledgment

The paper was completed with financial support from the National University Project (Code QG.11.07).

References

[1] H. J. Schulz, "Optical properties of 3d transition in II–VI compounds," *Journal of Crystal Growth*, vol. 59, pp. 65–80, 1982.

[2] Y. R. Lee, A. K. Ramdas, and R. L. Aggarwal, "Energy gap, excitonic, and internal Mn^{2+} optical transition in Mn-based II–VI diluted magnetic semiconductors," *Physical Review B*, vol. 38, no. 15, pp. 10600–10610, 1988.

[3] R. Y. Tao, M. M. Moriwaki, W. M. Becker, and R. R. Galazka, "Comporision of excitation spectra of 1.2 and 2.0 eV photoluminescence bands in Cd_{1-x} Mn_xTe for $0.4 < x < 0$," *Journal of Applied Physics*, vol. 53, no. 5, pp. 3772–3776, 1982.

[4] Y. Tanabe and S. Sugano, "On the absorption spectra of complex ions I and II," *Journal of the Physical Society of Japan*, vol. 9, pp. 753–767, 1954.

[5] A. Fazzio, M. J. Caldas, and A. Zunger, "Many-electron multiplet effects in the spectra of 3d impurities in heteropolar semiconductors," *Physical Review B*, vol. 30, no. 6, pp. 3430–3455, 1984.

[6] W. Chen, G. Li, J. O. Malm et al., "Pressure dependence of Mn^{2+} fluorescence in ZnS:Mn^{2+} nanoparticles," *Journal of Luminescence*, vol. 91, no. 3, pp. 139–145, 2000.

[7] W. Chen, R. Sammynaiken, Y. Huang et al., "Crystal field, phonon coupling and emission shift of Mn^{2+} in ZnS:Mn nanoparticles," *Journal of Applied Physics*, vol. 89, no. 2, pp. 1120–1129, 2001.

[8] S. Biswas, S. Kar, and S. Chaudhuri, "Optical and magnetic properties of manganese-incorporated zinc sulfide nanorods synthesized by a solvothermal process," *Journal of Physical Chemistry B*, vol. 109, no. 37, pp. 17526–17530, 2005.

[9] W. Chen, Z. Wang, Z. Lin, Y. Xu, and L. Lin, "Photoluminescence of ZnS clusters in zeolite-Y," *Journal of Materials Science and Technology*, vol. 13, no. 5, pp. 397–404, 1997.

[10] X. Fang and L. Zhang, "One dimensional (1D) ZnS nano materials and nanostructures," *Journal of Materials Science & Technology*, vol. 22, no. 6, pp. 721–736, 2006.

[11] Z. G. Chen, J. Jou, and D.-W. Weing, "Field emission and cathodoluminescence of ZnS hexagonal pyramids of zinc blende structured single crystals," *Advanced Functional Materials*, vol. 19, pp. 484–490, 2009.

[12] Y. C. Zhu, Y. Bando, and D. F. Xue, "Spontaneous growth and luminescence of zinc sulfide nanobelts," *Applied Physics Letters*, vol. 82, no. 11, pp. 1769–1771, 2003.

[13] D. Denzler, M. Olschewski, and K. Sattler, "Luminescence studies of localized gap states in colloidal ZnS nanocrystals," *Journal of Applied Physics*, vol. 84, no. 5, pp. 2841–2845, 1998.

[14] J. Nanda, S. Sapra, D. D. Sarma, N. Chandrasekharan, and G. Hodes, "Size-selected zinc sulfide nanocrystallites: synthesis, structure, and optical studies," *Chemistry of Materials*, vol. 12, no. 4, pp. 1018–1024, 2000.

[15] R. N. Bhargava, D. Gallagher, X. Hong, and A. Nurmikko, "Optical properties of manganese-doped nanocrystals of ZnS," *Physical Review Letters*, vol. 72, no. 3, pp. 416–419, 1994.

[16] N. Karar, F. Singh, and B. R. Mehta, "Structure and photoluminescence studies on ZnS:Mn nanoparticles," *Journal of Applied Physics*, vol. 95, no. 2, pp. 656–660, 2004.

[17] P. H. Borse, D. Srinivas, R. F. Shinde, S. K. Date, W. Vogel, and S. K. Kulkarni, "Effect of Mn^{2+} concentration in ZnS nanoparticles on photoluminescence and electron-spin-resonance spectra," *Physical Review B*, vol. 60, no. 12, pp. 8659–8664, 1999.

[18] W. Chen, A. G. Joly, J. O. Malm, and J. O. Bovin, "Upconversion luminescence of Eu^{3+} and Mn^{2+} in ZnS:Mn^{2+}, Eu^{3+} codoped nanoparticles," *Journal of Applied Physics*, vol. 95, no. 2, pp. 667–672, 2004.

[19] A. I. Cadiş, E. J. Popovici, E. Bica, I. Perhaiţă, L. Barbu-Tudoran, and E. Indrea, "On the preparation of Manganese-doped zinc sulphide nanocrystalline powders using the wet-chemical synthesis route," *Chalcogenide Letters*, vol. 7, no. 11, pp. 631–640, 2010.

[20] A. Twardowski, T. Dietl, and M. Demianiuk, "The study of the s-d type exchange interaction in $Zn_{1-x}Mn_xSe$ mixed crystals," *Solid State Communications*, vol. 48, no. 10, pp. 845–848, 1983.

[21] L. Levy, J. F. Hochepied, and M. P. Pileni, "Control of the size and composition of three dimensionally diluted magnetic semiconductor clusters," *Journal of Physical Chemistry*, vol. 100, no. 47, pp. 18322–18326, 1996.

[22] T. H. Ngo, H. van Bui, V. B. Pham et al., "Emission characteristics of SPAN-80 activated ZnS nanocolloids," *Journal of Luminescence*, vol. 132, pp. 2135–2142, 2012.

[23] D. Jiang, L. Cao, G. Su et al., "Synthesis and luminescence properties of ZnS:Mn/ZnS core/shell nanorod structures," *Journal of Materials Science*, vol. 44, pp. 2972–2975, 2009.